Spectrally-Efficient FM Noise Radar Waveforms Optimized in the Logarithmic Domain

Charles A. Mohr[1], Patrick M. McCormick[1], Shannon D. Blunt[1], Charles Mott[2]
[1]Radar Systems Lab (RSL), University of Kansas, Lawrence, KS
[2]Sensors Directorate, Air Force Research Laboratory (AFRL), Wright-Patterson AFB, OH

***Abstract*—It was recently experimentally demonstrated that spectrally-shaped FM noise waveforms can be designed that achieve very high time-bandwidth products and commensurately low sidelobes. While relatively good spectral containment can be obtained, increasing spectrum pressure may require that it be even better. To that end, here a logarithmic spectral shaping is performed by way of gradient-based optimization of a logarithmic frequency template error (Log-FTE) metric applied to a polyphase-coded FM (PCFM) waveform structure. Simulation and loopback experimental measurements show that this approach facilitates excellent spectral containment while still providing the high dimensionality and diversity benefits of FM noise waveforms.**

Keywords—FM noise radar, waveform optimization, spectral containment

I. Introduction

The noise radar concept has been around for many years [1] with a litany of contributions (e.g. [2-4]). Well known as a low probability of intercept (LPI) emission, noise radar does tend to be geared towards short-range applications due to the need for amplitude modulation (AM) and linear amplification. Until recently the notion of FM noise radar, which is not LPI but is amenable to high-power/long-range applications, had been limited to theoretical study [5]. However, its recent experimental demonstration [6,7] has opened the door for a variety of capabilities including practical spectral notching on transmit [8-10], tandem-hopped radar and communications [8,11], simultaneous dual-polarized emissions [12], a new form of nonlinear harmonic radar [13], mimicking the random spatial actuation of the human eye [14], and the practical implementation of complementary FM waveforms [15].

The FM noise waveforms originally developed in [6,7] and used in many of the subsequent extensions were designed by randomly initializing a polyphase-coded FM (PCFM) waveform [16] followed by an alternating projections optimization scheme operating in the time and frequency domains. In contrast, here we leverage a recent gradient-based formulation of PCFM optimization [17,18] that permits the use of a frequency-domain metric denoted as frequency template error (FTE) [19]. This metric is further modified by posing it in the logarithmic domain such that the resulting Log-FTE metric provides a natural basis with which to achieve very good spectral containment by virtue of emphasizing the spectral roll-off region equally with that of the passband.

The FTE and Log-FTE metrics are optimized within a gradient-descent structure that provides the means to design FM noise waveforms in an efficient manner using FFTs. Along with the previously developed pseudo-random optimized (PRO) FM noise waveforms, these new waveform sets are then evaluated in simulation and in an experimental loopback configuration. A simple example using a contrived image is also provided to assess the potential of FM noise waveforms for use in synthetic aperture radar (SAR).

II. Waveform Representation

The gradient-based optimization scheme used here operates on the PCFM implementation structure, which is a radar-oriented version of continuous phase modulation (CPM) used in communications. The first-order PCFM implementation can be expressed as [16]

$$s(t;\mathbf{x}) = \exp\left\{ j \left(\int_0^t g(\tau) * \left[\sum_{n=1}^{N} \alpha_n \, \delta\big(\tau - (n-1)T_p\big) \right] d\tau \right) \right\} , \quad (1)$$
$$= \exp\{ j\phi(t) \}$$

where $g(t)$ is a shaping filter with time support $[0, T_p]$, the operation $*$ represents convolution, $\delta(t)$ is an impulse function, and $\mathbf{x} = [\, \alpha_1 \; \alpha_2 \cdots \alpha_N \,]^T$ contains the set of phase-change parameters to optimize (akin to instantaneous frequencies). Because the operations comprising $\phi(t)$ are linear, this continuous phase function of time can alternatively be expressed as

$$\phi(t) = \sum_{n=1}^{N} b_n(t) \, \alpha_n \; , \quad (2)$$

where

$$b_n(t) = \int_0^t g(\tau - (n-1)T_p) \, d\tau \quad (3)$$

is the continuous basis function that is weighted by α_n. There are myriad other possible basis functions one could use such as higher-order PCFM [20] or Legendre polynomials [18]. Here we assume a rectangular shaping filter for $g(t)$ so that the resulting basis functions are time-shifted ramp functions.

To optimize these continuous waveforms, it is convenient to define a discretized version of $s(t)$ as

$$\mathbf{s} = \exp(j\mathbf{B}\mathbf{x}) \quad (4)$$

where the columns of $\mathbf{B}$ are discretized versions of $b_n(t)$. Thus $\mathbf{B}$ is an $M \times N$ matrix where N is the number of basis functions

This work was supported in part by the Office of Naval Research under Contract #N00014-16-C-2029 and by a subcontract with Matrix Research, Inc. for research sponsored by the Air Force Research Laboratory under Prime Contract #FA8650-14-D-1722. DISTRIBUTION STATEMENT A. Approved for Public Release.

and $M = KN$ is the length of $\mathbf{s}$ in samples, for K the factor of "over-sampling" relative to 3-dB bandwidth. This representation is equivalent to the discretized form in [16] in which N is approximately the time-bandwidth product (BT) for pulsewidth T and 3-dB bandwidth B.

To maximally utilize the available degrees of freedom for waveform design we also exploit the over-coding concept described in [21] such that the number of basis functions is instead set to $\tilde{N}$, which is greater than $N \cong BT$. Thus $\mathbf{B}$ becomes $M \times \tilde{N}$. For convenience we set $\tilde{N} = M$ so that $\mathbf{B}$ is a square matrix and then rely on the frequency domain cost function to ensure spectral containment.

III. Frequency Domain Metric

The frequency template error (FTE) metric was proposed in [19] as a means to optimize a waveform to achieve a desired power spectrum, inclusive of the spectral roll-off. A discretized version of the FTE metric can be expressed as

$$J_{\text{FTE}} = \left\| (\overline{\mathbf{s}}_{\text{f}}^{*} \odot \overline{\mathbf{s}}_{\text{f}}) - \mathbf{u} \right\| \tag{5}$$

where $\mathbf{u}$ is a length $2M-1$ discretized representation of the desired power spectrum template (all values real and positive), $(\bullet)^{*}$ indicates complex conjugation, and

$$\overline{\mathbf{s}}_{\text{f}} = \mathbf{A}^{H} \overline{\mathbf{s}} \tag{6}$$

is the length $2M-1$ Fourier transform of

$$\overline{\mathbf{s}} = [\mathbf{s}^{T} \ \mathbf{0}_{1\times(M-1)}]^{T} . \tag{7}$$

The $(2M-1) \times (2M-1)$ matrix $\mathbf{A}^{H}$ is a discrete Fourier transform (DFT) and $\mathbf{A}$ is the inverse DFT.

To compress the dynamic range, and thereby provide greater control over the degree of spectral containment, we can also pose (5) in the base-a logarithmic domain as

$$J_{\text{Log-FTE}} = \left\| \log_{a}(\overline{\mathbf{s}}_{\text{f}}^{*} \odot \overline{\mathbf{s}}_{\text{f}}) - \log_{a}(\mathbf{u}) \right\|, \tag{8}$$

with $\log_{a}(\bullet)$ being applied on an element-by-element basis. Note that (5) and (8) are implicitly defaulting to the $\ell = 2$ norm but any valid norm is possible.

The power spectrum template $\mathbf{u}$ used here is a Gaussian shape, which therefore corresponds to a Gaussian autocorrelation that theoretically possesses no sidelobes. Because frequency components with higher power contribute more to the overall error, the FTE metric of (5) tends to emphasize the passband of $\mathbf{u}$ over the spectral roll-off region, portions of which may be orders of magnitude lower than the passband. In contrast, the Log-FTE of (8) compresses the dynamic range of $\mathbf{u}$, thereby more evenly weighting the error from the passband and roll-off regions.

IV. Gradient-Based Optimization

For each randomly initialized PCFM waveform in the coherent processing interval (CPI), the FTE and Log-FTE functions were optimized using gradient descent. While there are myriad gradient-based formulations from which to choose, here we rely on the heavy ball approach [22]. The heavy ball method differs from standard steepest descent in that the descent direction is a linear combination of the current gradient and weighted versions of past gradients, thereby providing the descent direction an "inertia" much like a rolling heavy ball whose direction can only be changed slowly. For this method, the update of the phase-change code $\mathbf{x}$ is performed as

$$\mathbf{x}_{k+1} = \mathbf{x}_{k} + \mu_{k} \mathbf{p}_{k} , \tag{9}$$

where μ_{k} is the step-size and $\mathbf{p}_{k}$ is the current descent direction that is determined by

$$\mathbf{p}_{k} = \begin{cases} \boldsymbol{g}_{0} & \text{when } k = 0 \\ \boldsymbol{g}_{k} + \beta \mathbf{p}_{k-1} & \text{otherwise} \end{cases} \tag{10}$$

for $0 \le \beta < 1$. The step-size is chosen using a back-tracking method that satisfies the Wolfe conditions [23]. On occasion, $\mathbf{p}_{k}$ can become an ascent direction. In these cases, $\mathbf{p}_{k}$ is reset to the current gradient $\mathbf{g}_{k}$. This method was chosen because it converges much more quickly than steepest descent and was found to be more stable and requires fewer resets when compared to non-linear conjugate descent methods, particularly for the Log-FTE metric.

For gradient descent methods, the most computationally costly part of the algorithm is often the gradient calculation. The particular instantiations of the FTE metrics in (5) and (8) were formulated so that the gradient can be calculated using only FFTs and matrix-vector operations. This manner of fast gradient calculation was demonstrated in [24, 25] for phase codes and is extensible to PCFM-based gradients.

It can be shown that the gradients of (5) and (8) are

$$\nabla_{\mathbf{x}} J_{\text{FTE}} = \frac{2}{J_{\text{FTE}}} \overline{\mathbf{B}}^{T} \Im\left\{ \overline{\mathbf{s}}^{*} \odot \left[\mathbf{A}\left(\left\{ (\overline{\mathbf{s}}_{\text{f}}^{*} \odot \overline{\mathbf{s}}_{\text{f}}) - \mathbf{u} \right\} \odot \overline{\mathbf{s}}_{\text{f}} \right) \right] \right\} \tag{11}$$

and

$$\nabla_{\mathbf{x}} J_{\text{Log-FTE}} = \frac{2}{\ln(a) J_{\text{Log-FTE}}} \times \overline{\mathbf{B}}^{T} \Im\left\{ \overline{\mathbf{s}}^{*} \odot \left[\mathbf{A}\left(\left\{ \log_{a}(\overline{\mathbf{s}}_{\text{f}}^{*} \odot \overline{\mathbf{s}}_{\text{f}}) - \log_{a}(\mathbf{u}) \right\} \oslash \overline{\mathbf{s}}_{\text{f}}^{*} \right) \right] \right\} \tag{12}$$

respectively, where $\Im\{\bullet\}$ extracts the imaginary part, $\oslash$ is element-wise division, and

$$\overline{\mathbf{B}} = \left[\mathbf{B}^{T} \ \mathbf{0}_{\tilde{N}\times(M-1)} \right]^{T} \tag{13}$$

to account for the appended zeros in (7). Unsurprisingly, these gradients are very similar, with the only differences being the log operations and element-wise division by the spectrum conjugate in (12) rather than the element-wise multiplication by the spectrum in (11).

V. Simulation Results

We compare the design of FM noise waveforms using FTE and Log-FTE gradient-based optimization with the original pseudo-random optimized (PRO-FM) approach [6,7] that relies on alternating projections. The main difference between Log-FTE and the other two should be in the roll-off region. To evaluate performance, two different over-sampling factors were considered for the generation of 1000 FM waveforms of length $M = 900$. Each waveform was initialized by the first-order PCFM implementation [16], with random phase-change values

in **x** independently drawn from a uniform distribution on $[-\pi/K, +\pi/K]$. The over-sampling factors of $K = 3$ and 6 correspond to BT of 300 or 150, respectively. Each waveform was then optimized for 10^4 iterations using the gradient-based approach from Section IV.

The resulting matched filter responses were coherently combined to assess the zero-Doppler range sidelobes and average spectral content. For $K = 3$ (Fig. 1) there is a modest difference between the three approaches at the edges of the sampled bandwidth. The Log-FTE spectrum matches most closely to the Gaussian template in the roll-off region, while FTE provides the poorest match. There is a trade-off to be made for the improved spectral containment, however. Figure 2 illustrates the autocorrelation that results from coherently combining the 1000 matched filter responses at zero Doppler. While FTE and PRO-FM are nearly indistinguishable, the Log-FTE case realizes roughly 10-15 dB higher sidelobes.

For the $K = 6$ case the Gaussian template reaches a normalized power beyond −80 dB. However, this degree of spectral containment cannot be achieved by a square pulse shape and it has been observed that, as a result, the Log-FTE does not converge to acceptable waveforms. To address this issue while still maintaining constant amplitude waveforms (one could alternatively institute tapering) the Gaussian template was modified to possess a lower limit at −50 dB.

Figure 3 shows the average spectra for the three approaches for the higher degree of spectral containment that arises when $K = 6$. While the same ranking in performance is observed, the difference is now much more pronounced. The Log-FTE approach is able to match the desired spectrum to within 6-7 dB of the −50 dB lower bound, while FTE provides rather poor containment. An additional noteworthy effect of Log-FTE in this case is that it does not completely fill the available spectral content of the passband as specified by the Gaussian template, which occurs as a by-product of effectively equally weighting the importance between the passband and roll-off regions. The consequence of this effect can be observed in the associated autocorrelations in Fig. 4, where the mainlobe for Log-FTE is slightly wider. The Log-FTE sidelobes are once again about 10-15 dB higher as well.

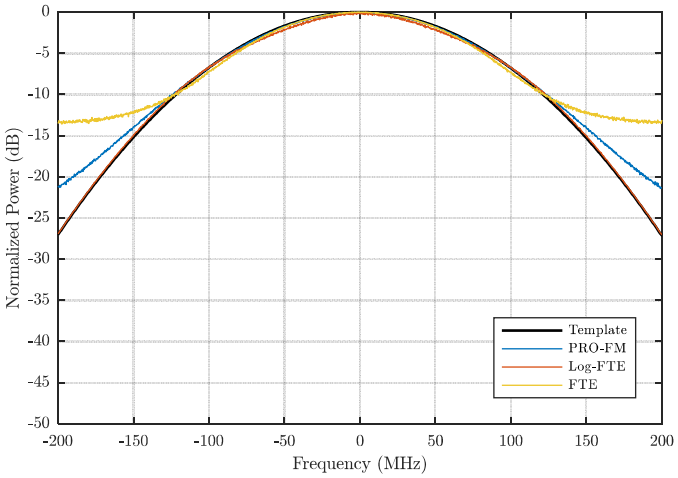

Fig. 1. Mean spectra for different FM noise design approaches ($K = 3$)

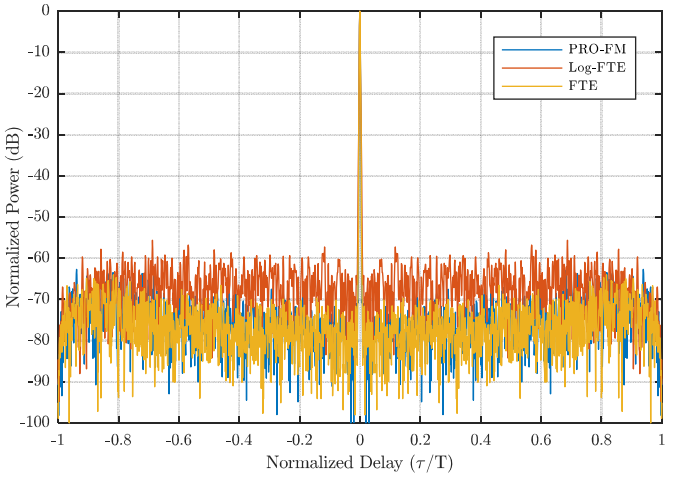

Fig. 2. Coherently combined autocorrelations for different FM noise design approaches ($K = 3$)

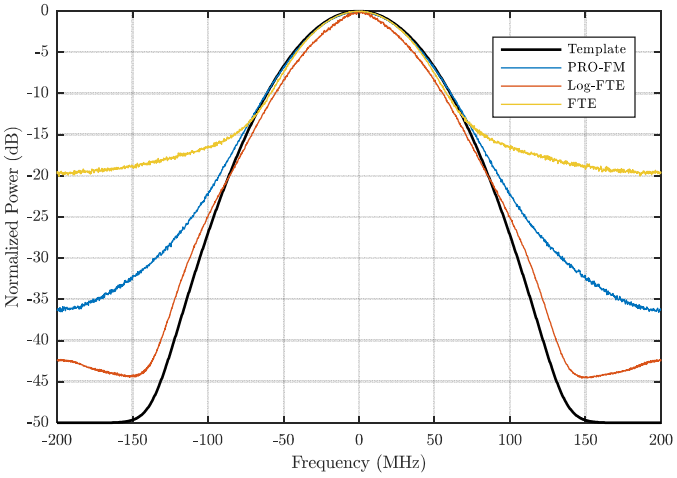

Fig. 3. Mean spectra for different FM noise design approaches ($K = 6$)

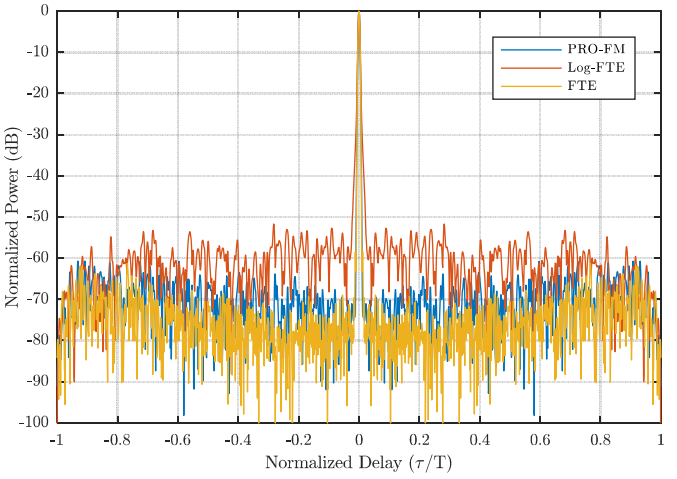

Fig. 4. Coherently combined autocorrelations for different FM noise design approaches ($K = 6$)

To demonstrate another useful facet of the Log-FTE optimization, an additional 1000 waveforms of length $M = 900$ were optimized using the three approaches to have a Gaussian spectrum containing a −50 dB notch in the passband. It has been previously observed [8] that PRO-FM is not capable of realizing a deep notch by itself and so it is supplemented with the Reiterative Uniform Weighting Optimizations (RUWO) algorithm [26] as demonstrated in [8,9]. The notch is likewise tapered as discussed in [9] to avoid the $\sin(x)/x$ range sidelobes that would otherwise arise.

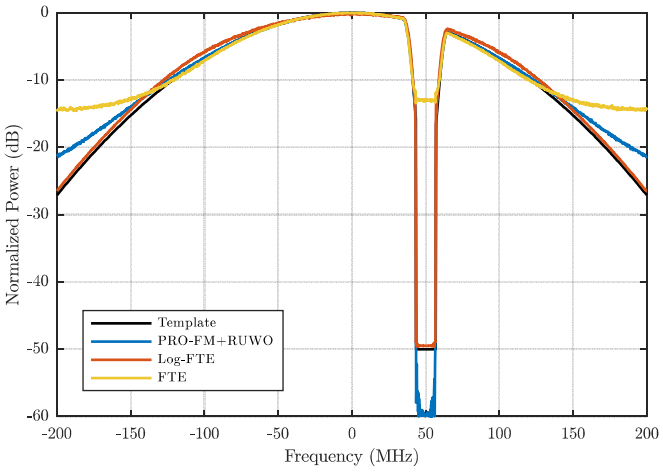

Fig. 5. Mean spectra for different FM noise design approaches ($K = 3$ and notched)

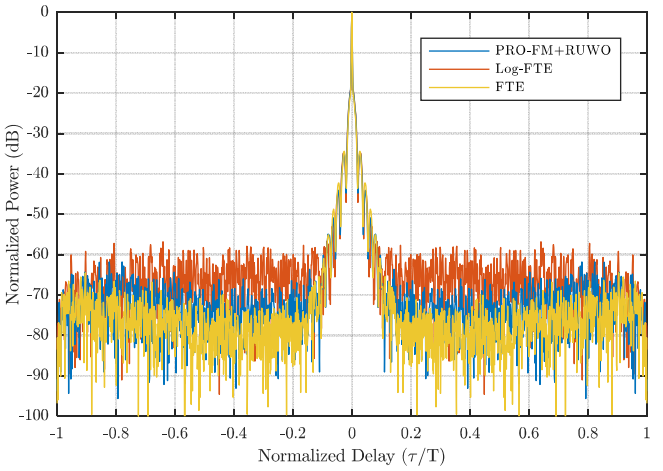

Fig. 6. Coherently combined autocorrelations for different FM noise design approaches ($K = 3$ and notched)

Figure 5 shows the resulting mean spectra for these different approaches along with the template. Like PRO-FM without RUWO (not shown), the FTE approach realizes a rather shallow notch depth of only about −13 dB. In contrast, the PRO-FM case with RUWO actually exceeds the specified notch depth because the RUWO method iteratively performs projections (alternated with enforcing constant amplitude). The Log-FTE approach still provides the closest fit to the Gaussian spectrum and likewise provides a near-perfect fit to the desired notch. The corresponding autocorrelations are illustrated in Fig. 6, where we see that the presence of the notch introduces shoulder lobes around the mainlobe, but with an otherwise similar response to the previously no-notched cases, which is the typical response that has been observed for notching of FM noise waveforms [27].

VI. Experimental Loopback Results

To verify the spectral containment behavior observed in simulation, the optimized waveforms were also evaluated experimentally in loopback. To do so, the waveforms were up-sampled from 200 MS/s to 10 GS/s and then digitally up-converted to a center of frequency of 3.55 GHz. The continuous signals were then generated by a Tektronix arbitrary waveform generator (AWG) with a 10 bit depth and subsequently passed through a (transmitter) amplifier, followed by an attenuator and low-noise (receiver) amplifier before being recorded on a Rhode & Schwarz FSW spectrum analyzer. The amplifiers and attenuators were included to mimic an open-air transmit and receive chain.

Figure 7 depicts the loopback measured spectra of the different design schemes for the $K = 3$ case. While these results now look almost identical to one another, note that it is the anti-aliasing filter of the RSA that is causing the sharp spectral cutoff. The loopback measurement of the $K = 6$ case (Fig. 8) is more meaningful since the 3 dB bandwidth is narrower and the RSA now passes a more significant portion of the roll-off spectrum. It is observed that the Log-FTE spectrum is the least affected in these loopback measurements, which is expected since it possesses the best spectral containment.

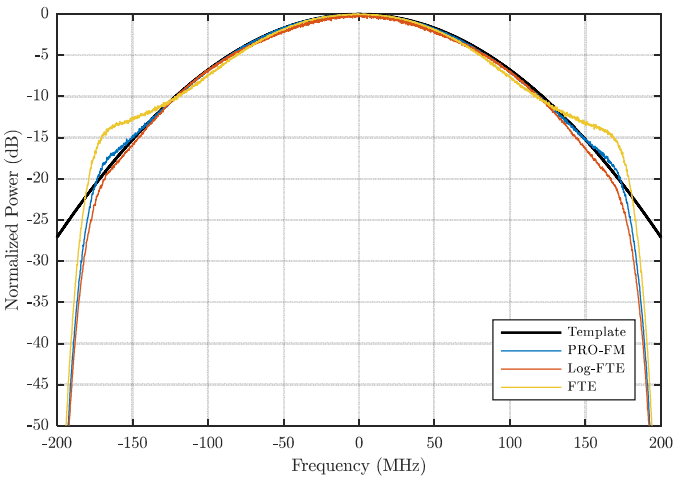

Fig. 7. Loopback measured mean spectra for different FM noise design approaches ($K = 3$)

Finally, the spectrally notched versions of the different FM noise design approaches were also assessed in loopback (Fig. 9). Here the PRO-FM/RUWO and Log-FTE cases both experience some degradation of the notch depth due to the small losses in waveform fidelity that are incurred by up-sampling (and thus interpolating) the waveforms for generation on the AWG and transmitter distortion. It is interesting to note that, though the difference is only about 1 dB, the Log-FTE notch depth is slightly better than PRO-FM/RUWO that explicitly used RUWO to facilitate deeper notches. Consequently, it is anticipated that the Log-FTE approach may ultimately provide

a more computationally efficient way to design these notched waveforms, which is absolutely essential for use in cognitive spectral avoidance applications (e.g. [10]) where real-time responsiveness is required.

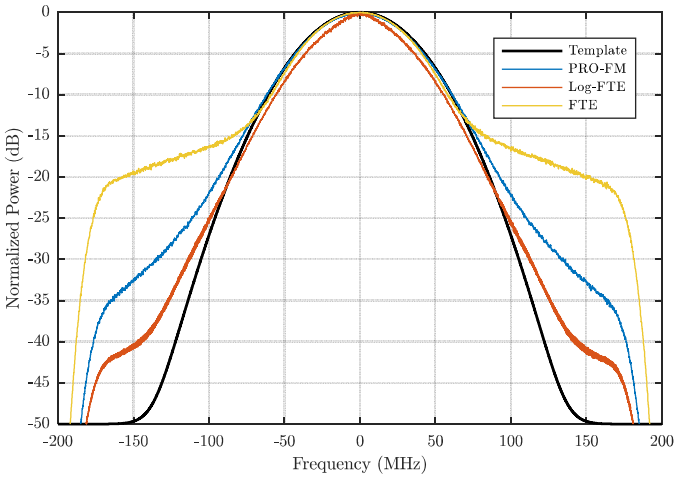

Fig. 8. Loopback measured mean spectra for different FM noise design approaches ($K = 6$)

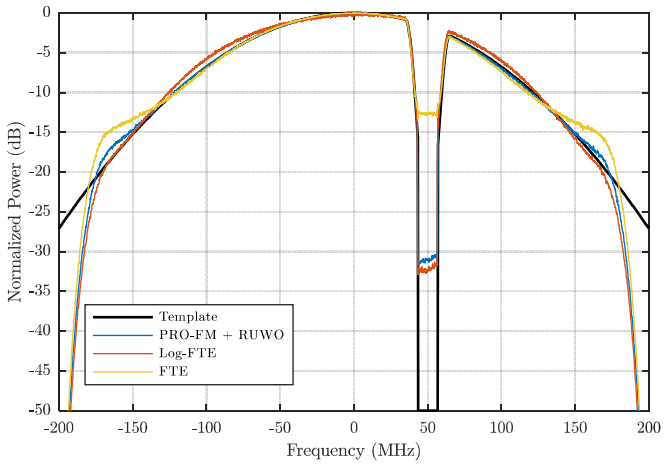

Fig. 9. Loopback measured mean spectra for different FM noise design approaches ($K = 3$ and notched)

While the bandlimiting effect of RSA anti-aliasing filter is clearly an imperfect representation of the true spectral content (and thus containment) of these waveforms, this result does draw attention to an important facet of spectral containment. The transmitter imparts distortion to the waveform that is both linear (i.e. a filtering operation) and nonlinear (predominantly from the power amplifier). While this distortion may be reduced through a variety of different predistortion and linearization methods (see [28,29]), a constant amplitude waveform that is spectrally well-contained goes a long way to mitigating these distortion effects as well. Minimal transmitter distortion and spectral containment will only become more important as the competition for radar spectrum continues to grow [30] and practical methods for radar/communication spectrum sharing are explored [31].

VII. SAR Application Example

Finally, FM noise waveforms provide their greatest benefit for applications in which the overall radar emission has high dimensionality. Synthetic aperture radar (SAR), which involves a CPI of many pulses of high BT, would therefore appear to be a possible good fit. To assess how these waveforms may perform for SAR, consider a simple simulation involving a clearly contrived image where the scatterers in range/azimuth are arranged in the shape of the University of Kansas logo. Each scatterer possessed an independently distributed random phase.

Using both a standard LFM waveform (of $BT = 128$) and Log-FTE FM noise waveforms with the same BT, back-projection was applied to the resulting simulated responses to form SAR images. Figure 10 illustrates the baseline LFM case and Fig. 11 depicts the Log-FTE FM noise waveform result.

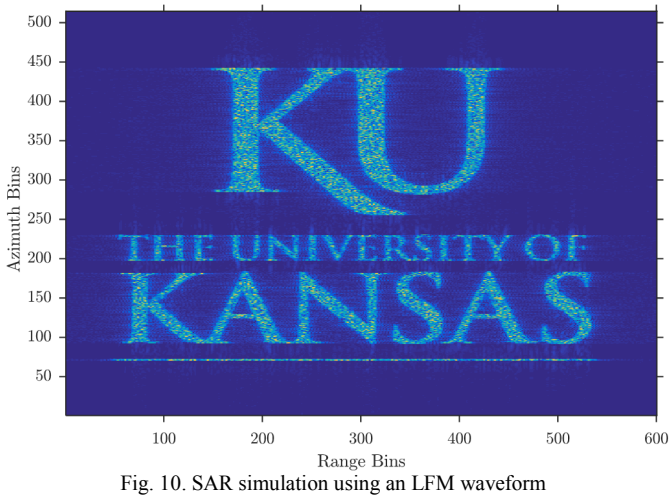

Fig. 10. SAR simulation using an LFM waveform

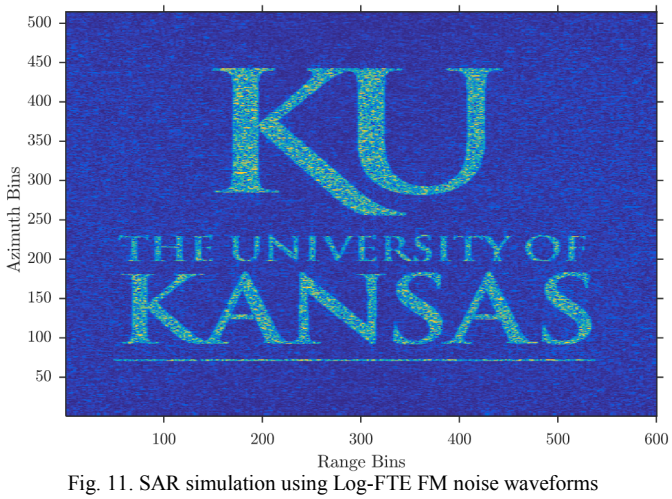

Fig. 11. SAR simulation using Log-FTE FM noise waveforms

The two most striking differences between Figs. 10 and 11 are the "fuzziness" of the edges in the LFM image and the higher background noise in the FM noise image. The former is due to the much higher sidelobes of the LFM waveform near the mainlobe, which could be reduced through tapering, filtering, or apodization, with an associated trade-off in degraded SNR or resolution. In contrast, the FM noise radar sidelobes are considerably lower following coherent combining

(as evidenced in Figs. 2 and 4) due to the fact that the differing sidelobes combine incoherently and thus realize an averaging effect. Of course, the trade-off in this case is a more evenly spread distribution of the remaining sidelobes in delay/Doppler, which is the cause for what appears to be background noise, though this effect could be driven lower given more pulses and/or higher *BT*. In short, while there still remains much to be examined, the pulse-agile nature of FM noise waveforms may lead to some interesting and potentially useful new trade-offs for SAR imaging.

VIII. Conclusions

A logarithm-based frequency template error (Log-FTE) cost function has been developed and applied to design FM noise waveforms within a gradient descent implementation. The Log-FTE optimization has been shown to produce waveforms that more closely match desired frequency templates that possess a high degree of spectral containment and that contain spectral notches. Of course, there is a practical limit to how well this containment can be achieved for constant amplitude waveforms. A simple SAR simulation was also used to illustrate the potential of such waveforms for high dimensionality radar modes.

References

[1] B.M. Horton, "Noise-modulated distance measuring systems," *Proc. IRE*, vol. 47, no. 5, pp. 821-828, May 1959.

[2] X. Xu, R.M. Narayanan, "Range sidelobe suppression technique for coherent ultra wide-band random noise radar imaging," *IEEE Trans. Antennas & Propagation*, vol. 49, no. 12, pp. 1836-1842, Dec. 2001.

[3] D. Tarchi, K. Lukin, J. Fortuny-Guasch, A. Mogyla, P. Vyplavin, A. Sieber, "SAR imaging with noise radar," *IEEE Trans. Aerospace & Electronic Systems*, vol. 46, no. 3, pp. 1214-1225, July 2010.

[4] M. Malanowski, K. Kulpa, "Detection of moving targets with continuous-wave noise radar: theory and measurements," *IEEE Trans. Geoscience & Remote Science*, vol. 50, no. 9, pp. 3502-3509, Sept. 2012.

[5] S.R.J. Axelsson, "Noise radar using random phase and frequency modulation," *IEEE Trans. Geoscience & Remote Sensing*, vol. 42, no. 11, pp. 2370-2384, Nov. 2004.

[6] J. Jakabosky, S.D. Blunt, B. Himed, "Waveform design and receive processing for nonrecurrent nonlinear FMCW radar," *IEEE Intl. Radar Conf.*, Arlington, VA, May 2015.

[7] J. Jakabosky, S. D. Blunt, B. Himed, "Spectral-shape optimized FM noise radar for pulse agility," *IEEE Radar Conf.*, Philadelphia, PA, May 2016.

[8] J. Jakabosky, S.D. Blunt, A. Martone, "Incorporating hopped spectral gaps into nonrecurrent nonlinear FMCW radar emissions," *IEEE CAMSAP Workshop*, Cancun, Mexico, Dec. 2015.

[9] J. Jakabosky, B. Ravenscroft, S.D. Blunt, A. Martone, "Gapped spectrum shaping for tandem-hopped radar/communications & cognitive sensing," *IEEE Radar Conf.*, Philadelphia, PA, May 2016.

[10] J. Owen, B. Ravenscroft, B. Kirk, S.D. Blunt, C. Allen, A. Martone, K. Sherbondy , "Experimental demonstration of cognitive spectrum sensing & notching," *IEEE Radar Conf.*, Oklahoma City, OK, Apr. 2018.

[11] B. Ravenscroft, P.M. McCormick, S.D. Blunt, J. Jakabosky, J.G. Metcalf, "Tandem-hopeed OFDM communications in spectral gaps of FM noise radar," *IEEE Radar Conf.*, Seattle, WA, May 2017.

[12] G. Zook, P.M. McCormick, S.D. Blunt, C. Allen, J. Jakabosky, "Dual-polarized FM noise radar," *IET Intl. Radar Conf.*, Belfast, UK, Oct. 2017.

[13] J. Owen, P. McCormick, S.D. Blunt, K. Gallagher, C. Allen, A. Martone, K. Sherbondy, "Nonlinear harmonic radar via intermodulation of FM noise waveform pairs," *IEEE Radar Conf.*, Oklahoma City, OK, Apr. 2018.

[14] G. Zook, P. McCormick, S.D. Blunt, "Spatial modulation driven by FM noise," *IEEE Radar Conf.*, Oklahoma City, OK, Apr. 2018.

[15] C. A. Mohr, P.M. McCormick, S.D. Blunt, T. Higgins, "Complementary waveform subsets within an FM noise radar CPI," *IEEE Radar Conf.*, Oklahoma City, OK, Apr. 2018.

[16] S. D. Blunt, M. Cook, J. Jakabosky, J. D. Graaf, E. Perrins, "Polyphase-coded FM (PCFM) radar waveforms, part I: implementation," *IEEE Trans. Aerospace & Electronic Systems*, vol. 50, no. 3, pp. 2218–2229, July 2014.

[17] P.M. McCormick, S.D. Blunt, "Nonlinear conjugate gradient optimization of polyphase-coded FM radar waveforms," *IEEE Radar Conf.*, Seattle, WA, May 2017.

[18] P.M. McCormick, S.D. Blunt, "Gradient-based coded-FM waveform design using Legendre polynomials," *IET Intl. Radar Conf.*, Belfast, UK, Oct. 2017.

[19] S.D. Blunt, J. Jakabosky, M. Cook, J. Stiles, S. Seguin, E.L. Mokole, "Polyphase-coded FM (PCFM) radar waveforms, part II: optimization," *IEEE Trans. Aerospace & Electronic Systems*, vol. 50, no. 3, pp. 2230–2241, July 2014.

[20] P.S. Tan, J. Jakabosky, J.M. Stiles, S.D. Blunt, "On higher-order representations of polyphase-coded FM radar waveforms," *IEEE Intl. Radar Conf.*, Arlington, VA, May 2015.

[21] J. Jakabosky, S. D. Blunt, and B. Himed, "Optimization of 'over-coded' radar waveforms," *IEEE Radar Conf.*, Cincinnatti, OH, May 2014.

[22] E. Ghadimi, R. Feyzmahdavian, M. Johansson, "Global convergence of the heavy-ball method for convex optimization," *European Control Conf.*, Linz, Austria, July 2015.

[23] J. Nocedal, S. Wright. Numerical Optimization, Springer Science & Business Media, 2006.

[24] B. O'Donnell, J.M. Baden, "Fast gradient descent for multi-objective waveform design," *IEEE Radar Conf.*, Philadelphia, PA, May 2016.

[25] D. Zhao, Y. Wei, Y. Liu, "Spectrum optimization via FFT-based conjuage gradient method for unimodular sequence design," *Signal Processing*, vol. 142, pp. 354-365, Jan. 2018.

[26] T. Higgins, T. Webster, A.K. Shackelford, "Mitigating interference via spatial and spectral nulling," *Radar, Sonar & Navigation, IET* , vol. 8, no. 2, pp. 84-93, Feb. 2014.

[27] B. Ravenscroft, S.D. Blunt, C. Allen, A. Martone, K. Sherbondy, "Analysis of spectral notching in FM noise radar using measured interference," *IET Intl. Radar Conf.*, Belfast, UK, Oct. 2017.

[28] F.H. Raab, P. Asbeck, S. Cripps, P.B. Kenington, Z.B. Popovic, N. Pothecary, J.F. Sevic, and N.O. Sokal, "Power amplifiers and transmitters for RF and microwave," *IEEE Trans. Microwave Theory & Techniques*, vol. 50, no. 3, pp. 814-826, Mar. 2002.

[29] F.M. Ghannouchi, O. Hammi, "Behavioral modeling and predistortion," *IEEE Microwave Magazine*, pp. 52-64, Dec. 2009.

[30] H. Griffiths, L. Cohen, S. Watts, E. Mokole, C. Baker, M. Wicks, S. Blunt, "Radar spectrum engineering and management: technical and regulatory issues," *Proc. IEEE*, vol. 103, no. 1, pp. 85-102, Jan. 2015.

[31] S.D. Blunt and E.S. Perrins, eds., *Radar & Communication Spectrum Sharing*, IET, 2018.